Identification of Ferroptotic Genes in Spinal Cord Injury at Different Time Points: Bioinformatics and Experimental Validation

Yu Kang
First Affiliated Hospital of Anhui Medical University
Qiangwei Li
Anhui Medical University
Rui Zhu
First Affiliated Hospital of Anhui Medical University
Shuang Li
First Affiliated Hospital of Anhui Medical University
Xin Xu
First Affiliated Hospital of Anhui Medical University
Xuanming Shi
Anhui Medical University
Zongsheng Yin (ahmu_zsyin@163.com)
First Affiliated Hospital of Anhui Medical University https://orcid.org/0000-0002-4862-5443

Research Article

Keywords: ferroptotic genes, spinal cord injury, bioinformatics, animal experiment

Posted Date: November 29th, 2021

DOI: https://doi.org/10.21203/rs.3.rs-1102903/v1

Abstract

Programmed cell death (PCD) is an important pathologic process after spinal cord injury (SCI), and as a newly type of PCD, ferroptosis is also involved in the secondary SCI, however, the underlying molecular mechanisms remain unclear. Integrating animal experiment and bioinformatics, we validated the ferroptotic phenotype in SCI first, and then bioinformatic analyses, including Gene Ontology enrichment analysis, Kyoto Encyclopedia of Genes and Genomes pathway analysis, gene set enrichment analysis and protein-protein interaction analysis were performed to investigate the ferroptotic genes at 1 day, 3 days, 7 days, 14 days and 56 days post-SCI, finally, the ferroptotic genes in SCI were identified and expression of 5 key genes were validated by western blot. The ferroptotic symbols including iron overload, lipid peroxidation, shrunken mitochondria and ROS accumulation were detected in the acute and sub-acute phase of SCI. The outcomes of bioinformatics suggested that mTOR signaling pathway, HIF-1 signaling pathway, VEGF signaling pathway, Protein processing in endoplasmic reticulum were involved in ferroptotic regulation and ATF-3, XBP-1, HO-1, DDIT-3 and CHAC-1 were selected as the ferroptotic key genes in SCI. Besides, response to oxidative stress, amide metabolic process, cation transport and cytokine production were showed as the essential biological process in ferroptosis after SCI. The ferroptotic phenotype following SCI was validated and the ferroptotic genes and signaling pathways were identified. The results contribute to exploring the ferroptotic mechanism underlying secondary SCI and to providing potential target for clinical treatment.

Introduction

Spinal cord injury (SCI) is a severe central nervous system injury that results in irretrievable loss of sensory and motor function below the site of injury[1]. The pathophysiology of SCI can be divided into primary and secondary injury [2]. Primary injury is the initial trauma caused by mechanical contusion or extrusion. Secondary injury refers to the multifaceted pathological process that includes tissue edema, inflammatory reaction, necrosis, and programmed cell death (PCD) etc following primary injury[3]. As the large hurdles of neural regeneration in SCI, PCD has attracted increasing attention in recent years[4, 5, 6], nevertheless, the molecular mechanism remains inconclusive.

Ferroptosis was proposed by Dixon et al. in 2012 [7]. Just as its name implies, ferroptosis was a new form of PCD mediated by ferric ion while differ from apoptosis, necrosis, and autophagy etc [8]. Symbol of ferroptosis, such as overloaded iron, shrunken mitochondria, accumulated lipid peroxidation and upregulated ROS, have been observed in animal models of SCI, and this process can be reversed by ferroptosis inhibitors such as deferoxamine (DFO) and SRS 16-86 [9, 10, 11]. Above studies revealed that ferroptosis played an important role in SCI. Therefore, a comprehensive analysis of the ferroptotic genes in SCI contributes to a deeper understanding of secondary SCI and to seeking new therapeutic targets.

GEO (Gene expression Omnibus) is an international public repository that archives and freely distributes microarray, next-generation sequencing, and other forms of high-throughput functional genomics data submitted by the research community[12]. FerrDb, the first database of ferroptosis, was constructed by Nan Zhou et al. in 2019 [13]. There are six data sets in FerrDb including Marker, Driver, Suppressor, Inducer, Inhibitor and Ferroptosis-disease association. Based on GEO and FerrDb, the interaction of SCI and ferroptosis can be analyzed by bioinformatic methods.

In this study, we verified the ferroptotic phenotype via testing the levels of tissue iron, Malondialdehyde (MDA) and reactive oxygen species (ROS), and observing mitochondrial morphology. Subsequently, the datasets derived from GEO and FerrDb were used to capture differentially expressed genes (DEGs) related with ferroptosis at different time points (1 day/3 days /7 days /14 days /56 days) of SCI. DEGs of every time point gone through the Gene Ontology (GO) functional annotation analysis and Kyoto Encyclopedia of Genes and Genomes (KEGG) pathway enrichment analysis and gene set enrichment analysis (GSEA). The protein-protein interaction (PPI) networks were established and the ferroptotic hub genes in SCI were identified. (Figure 1).

Materials And Methods

Animal Groups and SCI Model

Female Sprague-Dawley (SD) rats (Anhui Medical University) were chosen as the experimental animal in the present study (8-10 weeks old, weighing 230-260 g). All rats were housed under a 12 h light/dark cycle pathogen-free condition with a controlled temperature of 24 ± 2 °C and 60 ± 5% humidity and free access to food and water. All experiments and procedures were performed in accordance with the National Institutes of Health (NIH) Guide for the Care and Use of Laboratory Animals. The study protocols

regarding the animals were approved by the Ethics Committee of Anhui Medical University of China (No.LLSC 20201135). All rats were divided into three groups: Sham, SCI_Day 3 and SCI_Day 14.

The SCI model was induced via modified version of Allen's method as described previously[14]. Animals were anesthetized by 10% chloral hydrate (3 ml/kg, intraperitoneal injection). When the corneal reflex disappeared, T10 laminectomy was performed to expose the spinal cord under an aseptic condition. Subsequently, the rats in SCI group underwent a surgery using an impactor (10 g weight × 5 cm height) to induce T10 spinal cord injury and the rats in sham group were accepted the T10 laminectomy only. The bladder was evacuated manually twice a day until bladder function was recovered.

Behavioral Assessment for SCI

The classical Basso, Beattie and Bresnahan (BBB) scale was used here for the behavioral assessment[15]. BBB scale ranges from 0 to 21 points, which means complete hindlimb disability and normal locomotor function. Rats were assessed to evaluate locomotor function 30 min preoperatively and 1, 3, 7 and 14 days postoperatively. To avoid experimental errors, the rats should be allowed to move freely for 5 minutes in the open filed before every evaluation. To avoid bias results, assessments were executed by three researchers that were blinded to animal groups.

Hematoxylin-Eosin, Nissl and Perls-Blue Staining

Necrosis cavity, number of motor neurons and iron accumulation was observed via HE, nissl and perls-blue staining severally. The rats were sacrificed and one centimeter of the SCI tissue was removed, 5mm to the rostral and caudal centered around epicenter lesion. Then the specimens went through the steps that included fixation, dehydration, embedded, section (horizontal sections, thickness 4 μm) and incubation (65℃ for 20 minutes). After incubation, slices were stained by hematoxylin-eosin, nissl staining solution with cresyl violet (G1430, Solarbio) and prussian blue iron stain kit with nuclear fast red solution (G1422, Solarbio) respectively.

Transmission Electron Microscope

Rats were perfused with transmission electron microscope (TEM) fixation liquid (Paraformaldehyde 2% - Glytaraldehyde 2.5% in PBS, P885738, Macklin). Epicenter lesion samples were collected from removed spinal cords cut into sections (70-90 nm). After post-fixed in 2% osmium tetroxide, dehydrated in ethanol and then embedded in eponate, sections were placed on a copper mesh and stained with 2% uranyl acetate and 0.04% lead citrate. These sections were observed and imaged with TEM (Talos L120C G2, Thermo Scientific).

Iron and MDA Concentration Test

Iron accumulation in SCI was tested using the tissue iron assay kit (A039-2-1, Nanjing Jiancheng Bioengineering Institute). Malondialdehyde (MDA), as a natural product of lipid peroxidation, was quantified using Lipid Peroxidation MDA Assay Kit (S0131S, Beyotime). The protocols of iron and MDA concentration tests were performed according to the menufacturer's instructions and the absorbance was measured at 532 nm and 520 nm respectively.

ROS assay

ROS production was determined by chemiluninescence using the fluorescent probe 2', 7'-dichlorodihydrofluorescein diacetate (DCFH-DA, WanleiBio). After anesthetization, rats were perfused transcardially with precooled PBS and the spinal cords were digested by pancreatin to obtain single-cell suspensions. Cells were incubated with DCFH-DA (10 μM) at 37℃ for 20 minutes. Later, the cells were observed and pictured via the inverted fluorescence microscope (Axio Observer 3, Germany). The ROS fluorescence intensity was calculated by software Image J.

Protein Extraction and Western Blot Test

The isolated spinal cords were homogenated with RIPA buffer (Beyotime Biotechnology, Shanghai, China) containing 1% protease inhibitor (Beyotime Biotechnology, Shanghai, China) for 30 minutes on ice. The homogenates were centrifuged at 12000 g for 25 minutes at 4°C and supernatants were collected. NanoDrop 2000C (Thermo Scientific, USA) was then used for protein concentrations determination. The homogenates and loading buffer 5× (Beyotime Biotechnology, Shanghai, China) were mixed at a ratio of 4: 1,

denatured in the metal bath (100°C, 8~10 mins), cooled to room temperature and loaded. Protein samples were subjected to 12.5% SDS-PAGE (Epizyme Biotech, Shanghai, China) and then transferred to polyvinylidene fluoride (PVDF) membranes. Membranes were blocked in protein free rapid blocking buffer (Epizyme Biotech, Shanghai, China) for 15 minutes at room temperature. After blocking, membranes were incubated with the primary antibodies against ATF3 (DF6660, Affinity Biosciences), XBP1 (WL00708, WanleiBio), HMOX1 (WL02400, WanleiBio), DDIT3 (GADD153, Proteintech), CHAC1 (DF9353, Affinity Biosciences) and GAPDH (AF7021, Affinity Biosciences) overnight at 4°C. Membranes were incubated with the secondary antibody at room temperature for 1.5 h. Protein bands were captured using an ECL chemiluminescence system (Epizyme Biotech, Shanghai, China).

Statistical Analysis

Statistical analysis and graphs were both performed by GraphPad Prism 8.0 software. BBB scores comparisons were analyzed by LSD t-test. Iron content, MDA content and ROS fluorescence intensity comparisons were analyzed using one-way analysis of variance (ANOVA). $P < 0.05$ indicated that the difference was statistically significant.

Data Source

The microarray expression profiling dataset GSE45006 was download from the GEO database (https://www.ncbi.nlm.nih.gov/geo/). The gene sets of ferroptosis markers and regulators were download from FerrDb (http://www.zhounan.org/ferrdb/). GSE45006 was based on GPL1355 [Rat230_2] Affymetrix Rat Genome 230 2.0 Array. GSE45006 contained 24 samples consisting of 4 intact spinal cords and 20 injured spinal cords that were from different time points. We grouped the injured spinal cords by 1day, 3days, 7 days, 14 days and 56 days and the 4 intact spinal cords were defined as control group.

Analysis of DEGs

We used GEO2R (https://www.ncbi.nlm.nih.gov/geo/geo2r/) to compare samples of control group and 5 injured groups in order to identify genes that are differentially expressed at different time point after SCI. Genes obtained from GEO2R were screened by following criteria: (1) adjusted P-value < 0.05 and (2) $|logFC| \geq 0.5$. The intersecting part of screened genes and ferroptosis makers was identified using the Venn diagram webtool (http://bioinformatics.psb.ugent.be/webtools/Venn/) and this part was considered as DEGs.

GO and KEGG Enrichment Analysis of DEGs

The Database for Annotation, Visualization and Integrated Discovery (DAVID v6.8, https://david.ncifcrf.gov/home.jsp) was used in this step to carry the Gene Ontology (GO) functional enrichment analysis on DEGs[16]. The GO annotation analysis was focused on biological process (BP), molecular function (MF), and cellular component (CC)[17]. Kyoto Encyclopedia of Genes and Genomes (KEGG) pathway enrichmennt analysis was performed using the KOBAS online tool (http://kobas.cbi.pku.edu.cn/)[18]. Adjusted P-value < 0.05 was considered as the cutoff criteria. Bar charts of GO enrichment analysis were visualized by “ggplot2” package of R software, GOChord plot and the bubble plot for KEGG enrichment analysis was produced by http://www.bioinformatics.com.cn, a free online platform for data analysis and visualization.

Gene Set Enrichement Analysis

Gene set enrichment analysis (GSEA) was performed for all time points to prevent loss of ferroptotic genes that were out of threshold we set but crucial to SCI. All the ferroptosis marker genes of each time point were defined as the target gene set. Background gene set was combination of KEGG and GO (BP, MF, CC) gene sets. An absolute value of the standardized enrichment score (NES) > 1 and p-value < 0.05 was taken as the cutoff criteria of statistical significance[19, 20, 21]. Packages “org. Rn.eg.db”, “ClusterProfiler”, “enrichplot”, “gseaplot2” of R software were used for GSEA analysis and visualization.

PPI Network Analysis and Hub Gene Identification

STRING (https://string-db.org/) is a database of known and predicted protein-protein interactions that include direct (physical) and indirect (functional) associations[22]. We used the STRING to construct the PPI network of DEGs under the condition that combined score of PPI pairs was greater than 0.4. Visualization of PPI network was completed via Cytoscape software v3.7.2 (www.cytoscape.org)[23]. CytoHubba, a plugin in Cytoscape software, can predict and explore important nodes and subnetworks in a

given network by several topological algorithms. We used CytoHubba to calculate the MCC score of each protein node and top six genes were identified as hub genes.

Selection of Key Genes for Ferroptosis Regulation in SCI

We focused on the links between differentially expression and ferroptosis regulation of hub genes obtained from 1 day, 3 days, 7 days, 14 days and 56 days. The hub genes that exist in acute phase, sub-acute phase and chronic phase of SCI were identified as the key genes. The regulating effect of the key genes in the process of ferroptosis were checked in the Ferroptosis driver, suppressor and marker dataset downloaded from FerrDb. The function of key genes were annotated by the GeneCard database (https://www.genecards.org/).

Results

Validation of Ferroptosis following SCI

Ferroptosis is characterized by iron accumulation, shrunken mitochondria and lipid peroxidation. Here we constructed SCI animal model by modified Allen's method and verified the feasibility of the model through HE and nissl staining and BBB scale. BBB scores of SCI group were significant lower than sham group at 1 day, 3 days, 7 days and 14 days (**Figure 2D**). HE staining showed the apparently cavity in both SCI_3 days and SCI_14 days (**Figure 2A**). Nissl staining depicted that the number of motor neurons were decreasing after SCI (**Figure 2B**). Meanwhile, ultrastructure of the spinal cord was observed using TEM. The normal mitochondria were observed in the sham group while mitochondria in these 2 SCI groups had shrunken (**Figure 3A**). Then we used perls-blue staining and tissue iron assay kit to verified the upregulation of iron ion after SCI. Iron content of SCI_3 days (25.07 ± 2.70 nmol/mg) and SCI_14 days (38.64 ± 3.64 nmol/mg) were both greater than sham (15.51 ± 2.28 nmol/mg), which accorded with the result of perls-blue staining (**Figure 2C,E**). Lipid peroxidation MDA assay kit and DCFH-DA were used to evaluated the peroxidation status. After SCI, the MDA concentration was increased and the augmented level of ROS was presented and quantified in **Figure 3B-D**.

Identification of DEGs

The gene expression profiles GSE45006 was selected in this study. GSE45006 contained 20 SCI samples (1 day /3 days /7 days /14 days /56 days, n=4) and 4 normal samples. There were 4093, 3443, 3044, 2390, 2699significant upregulated genes and 3594, 2909, 2538, 1893, 2090 significant downregulated genes at 1 day, 3 days, 7 days, 14 days and 56 days after SCI respectively (adjusted $P < 0.05$). In the volcano plot, every plot indicated a gene and the blue plots were downregulated, the red plots was upregulated (**Figure 4A**). The boxplot showed that the medians of each sample data were almost at the same level, which means that the data met the standard for further analysis (**Figure 4B**). Among the upregulated and downregulated genes obtained previously, we screened out the ones satisfied with the criteria of $|logFC| \geq 0.5$ and Venn analysis was performed to get the intersection of these genes and ferroptosis marker dataset (**Figure 4C**). Ferroptosis marker dataset was downloaded from FerrDb and contained 123 annotated genes with 137 genes symbols (14 genes with two different symbols). Finally, ferroptosis-related DEGs of 5 time points after SCI was obtained for subsequent analysis (**Table 1**).

GO Functional Enrichment Analysis

GO functional enrichment analysis was performed using the DAVID 6.8 and visualized by using R software and the bioinformatic online tool. The eligible terms for GO analysis of each time point were shown in **Figure 5**. We listed the GO terms in **Supplementary Table 1** according to the different phases of SCI (Day1, 3 and 7 were acute phase, Day 14 was sub-acute phase and Day 56 was chronic phase)[24]. We picked out 7 GO terms related to ferroptosis (**Supplementary Table 2**): cellular response to oxidative stress, positive regulation of transcription from RNA polymerase II promoter in response to oxidative stress, response to oxidative stress, cellular oxidant detoxification, cellular response to hydrogen peroxide, positive regulation of cell death, mitochondrion, the genes enriched in these terms were shown in **Figure 6**.

KEGG Pathway Enrichment Analysis

KEGG pathway enrichment analysis was performed using the KOBAS database and visualized by using the bioinformatic online tool. We arranged KEGG terms in ascending order of adjusted-P values at each time point, top ten terms were remained and visualized in **Figure 7**. Afterwards, we filtered these terms further and the terms that throughout the three phases of SCI were mTOR signaling

pathway, HIF-1 signaling pathway, Ferroptosis, VEGF signaling pathway and Protein processing in endoplasmic reticulum. Details of these KEGG terms were shown in **Table 2**. Totally 69 different pathways with adjusted-P value less than 0.05 were enriched in 5 time points (**Supplementary Figure 1**).

Gene Set Enrichment Analysis

Further detecting of regulative genes and involved signaling pathways in ferroptosis after SCI at each time points was performed by GSEA (**Figure 8**). The pathways that were not enriched in analysis of DEGs were emerged: inflammatory response, cation transport, positive regulation of catabolic process, oxidoreductase activity, cytokine mediated signaling pathway, amide biosynthetic process, signaling receptor binding, leukocyte migration, enzyme binding et al. Meanwhile, some of the ferroptosis marker genes excluded in screening DEGs were discovered in the leading edge subset of GSEA: *ALOX15, SLC1A4, SLC7A11, HSPB1, PTGS2, GPX2, RELA, EIF2S1, DUSP1, HIC1, SLC7A5, YWHAE, OXSR1, IREB2, DDIT3, KLHL24, ATF4, MAPK14, MAFG* (**Figure 9**).

Establishment of PPI Network

PPI network analysis was performed by the STRING database and the software Cytoscape (version 3.7.2) was used for visualization of PPI network. The PPI network of Day 1 contained 24 nodes (18 upregulated genes, 6 downregulated genes) and 49 linkages. The PPI network of Day 3 contained 33 nodes (26 upregulated genes, 7 downregulated genes) and 97 linkages. The PPI network of Day 7 contained 17 nodes (15 upregulated genes, 2 downregulated genes) and 25 linkages. The PPI network of Day 14 contained 19 nodes (12 upregulated genes, 7 downregulated genes) and 39 linkages. The PPI network of Day 56 contained 22 nodes (16 upregulated genes, 6 downregulated genes) and 53 linkages. (**Figure 10A**)

Identification of Hub Genes

The top six genes of each time point were calculated by MCC algorithm of CytoHubba and the results were shown in Fig 10B. The hub genes in Day 1 were *HMOX1* (score=26), *VEGFA* (score=17), *ATF3* (score=16), *PTGS2* (score=14), *NFE2L2* (score=12), *XBP1* (score=9). The hub genes in Day 3 were *ATF3* (score=912), *ATF4* (score=894), *DDIT3* (score=888), *XBP1* (score=870), *ASNS* (score=768), *CHAC1* (score=727). The hub genes in Day 7 were *VEGFA* (score=11), *HMOX1* (score=10), *XBP1* (score=7), *ATF3* (score=6), *RELA* (score=4), *BNIP3* (score=4). The hub genes in Day 14 were *VEGFA* (score=26), *ATF3* (score=25), *DDIT3* (score=23), *XBP1* (score=22), *HMOX1* (score=11), *CHAC1* (score=18). The hub genes in Day 56 were *ATF4* (score=116), *ATF3* (score=98), *DDIT3* (score=97), *XBP1* (score=80), *HMOX1* (score=68), *CHAC1* (score=31).

Selection and Validation of Key Genes for Ferroptosis in SCI

There were 12 different gene symbols in the hub genes: *ATF3, XBP1, HMOX1, VEGFA, ATF4, NFE2L2, PTGS2, DDIT3, ASNS, CHAC1, RELA, BNIP3*. Selection of key genes depended on whether time point distribution of the hub gene covered the three phases (acute: Day 1, 3, 7, sub-acute: Day 14, chronic: Day 56) of SCI. Among the hub genes, 5 genes were identified as the key genes for ferroptosis in SCI: *ATF3, XBP1, HMOX1 (HO-1), DDIT3, CHAC1*. Functional description, regulation effect on ferroptosis and expression of key genes were presented in **Table 3**. Additionally, expression levels of key genes were validated via western blot test of which results were in line with the consequences yielded from bioinformatic analysis (**Figure 11**).

Discussion

Bioinformatic analysis was an important means of exploring the complex molecular mechanism of SCI. A previous bioinformatic study found that ANXA1, SNAP25 and SPP1 were closely related to spinal cord repair and regeneration after injuried[17]. A sequence analysis of SCI revealed the effect of noncoding RNA in SCI and a ceRNA regulation network with miR-21 as the center was constructed[25]. Recently, a research combined with proteomics and bioinformatics indicate that the protein module continuously upregulated at the acute and subacute time points after SCI was associated with the lipid regulation[26]. Alternatively, a increasing number of studies focused on the ferroptosis following SCI in recent years. It was reported that proanthocyanidin could inhibit ferroptosis and promoted functional recovery of SCI[27]. Zinc was found to improve the recovery of SCI via upregulating the expression of NRF2 and GPX4 that could attenuate ferroptosis[28]. Although it has been demonstrated that adjustion of ferroptosis could affect the recovery of SCI, the specific pathways and genes were still unclear. Consequently, a bioinformatic analysis targeting on ferroptosis in SCI was performed here to investigate the core factors of regulation.

This study combined both animal experiment and bioinformatic analysis in order to validate the existence of ferroptosis and identify the ferroptotic genes in SCI. We primarily examined the symbols of ferroptosis following SCI, including morphological structure of mitochondria, overloaded iron, lipid peroxidation and reactive oxygen species. Shrunken mitochondria were observed via TEM at 3 days and 14 days after SCI. Iron accumulation in SCI was verified by the tissue iron assay kit whose results were consist with the perls-blue staining. Elevated MDA content and higher level of ROS suggested the peroxidation status of cells in SCI. For bioinformatic analysis, two datasets (GSE45006 and Ferroptosis Marker dataset) were downloaded to screen DEGs related ferroptosis at different time point after SCI. Among the genes that met the cutoff criteria, we found 37 ferroptosis markers at Day 1, 43 ferroptosis markers at Day 3, 28 ferroptosis markers at Day 7, 28 ferroptosis markers at Day 14 and 32 ferroptosis markers at Day 56. These markers considered as DEGs underwent a series of analyses subsequently. Eventually, ferroptosis-related hub genes, signaling pathways and key genes were yielded from the analyses. Discovery of these genes and pathways provide insight into the pathophysiology of SCI.

GO enrichment analysis showed that the DEGs were mainly involved in cell response to hypoxia and oxidative stress, the regulation of programmed cell death (PCD), mitochondrion function, transcription factor activity, DNA/protein binding, protein homodimerization activity, blood vessel endothelial cell migration. Among these GO terms, there were 7 ferroptosis-related terms enriched with 25 genes. KEGG pathway enrichment analysis suggested that the DEGs were primarily involved in mTOR signaling pathway, VEGF signaling pathway, Mitophagy, IL-17 signaling pathway, Metabolic pathways, HIF-1 signaling pathway, TNF signaling pathway, Ferroptosis, Protein processing in endoplasmic reticulum, Cytosolic DNA-sensing pathway and MAPK signaling pathway. Among these KEGG terms, 5 signaling pathways were enriched in acute, subacute and chronic phases of SCI: mTOR signaling pathway, HIF-1 signaling pathway, Ferroptosis, VEGF signaling pathway and Protein processing in endoplasmic reticulum. Results of GSEA supplemented that cation transport, cytokine mediated signaling pathway, amide biosynthetic process were also worthy to be focused in SCI.

The mammalian target of rapamycin (mTOR) signaling pathway plays an important role in trauma and various diseases in the central nervous system (CNS)[29]. Modulation of mTOR signaling pathway can improve motor recovery via restraint of inflammation and apoptosis after SCI[30]. Furthermore, as a negative autophagy regulator, mTOR signaling pathway is implicated in regulating autophagy-dependent ferroptosis[31].

Hypoxia inducible factor-1 (HIF-1) signaling pathway is involved in the cellular response to hypoxia. Elevation expression of HIF-1 benefits neurological recovery in SCI rats[32, 33]. And the negative effect of HIF-1 on ferroptosis was implemented via inducing transcription of fatty acid binding protein 3 and fatty acid binding protein 7[34].

The primary function of vascular endothelial growth factor(VEGF) signaling pathway is associated with angiogenesis. VEGF may indirectly protect the nerve from ischemic and anoxic injury and activation of HIF-1/VEGF signaling pathway contributes to recovery from SCI[35]. Evidence of the cross-talk between VEGF and ferroptosis signaling pathway was that overexpression of VEGF was detected in retinal pigment epithelium (RPE) cells treated with H_20_2 and the production of VEGF was inhibited by the ferroptosis suppressor SLC7A11[36].

Endoplasmic Reticulum (ER) is vital for redox balance of cells. Persistant exposure to excessive stress drives the ER-associated cell death pathway[37]. Recently, a new research presented that ER stress was crucial for blood-spinal cord barrier (BSCB) disruption after SCI and inhibition of ER stress contributed to the integrity of BSCB[38]. As a regulator of lipid homeostasis, ER is closely related with ferroptosis[39]. Unfolded protein response (UPR), the adaptive mechanism for ER homeostasis, is affected by ferroptotic regulators such as erastin[40], xCT[41], ATF4[42], NRF2[43].

PPI networks of each time point were constructed and the hub genes were identified via CytoHubba based on MCC algorithm. There were total 12 hub genes at 5 time points: *ATF3, XBP1, HMOX1, VEGFA, ATF4, NFE2L2, PTGS2, DDIT3, ASNS, CHAC1, RELA, BNIP3*. Among these genes, *ATF3, XBP1, HMOX1, ATF4, NFE2L2, PTGS2, DDIT3, ASNS, RELA* were upregulated, *VEGFA* and *BNIP3* were downregulated, *CHAC1* was upregulated at Day 3 while downregulated at Day 14 and Day 56. Furtherly, 5 genes were found differentially expressed in all three phases following SCI: *ATF3, XBP1, HMOX1 (HO-1), DDIT3* and *CHAC1*.

Activation transcription factor 3 (ATF3) is a member of the ATF/CREB family of transcription factors, and it is induced under a wide range of stress condition, including cell injury and oxidative stress[44]. A previous study showed that ATF3 was upregulated after SCI in rats and expression of NeuN was declined with AFT3 expressing in cells[45]. On the other hand, ATF3 was reported to suppress the system Xc- via binding to the SLC7A11 promoter and inhibiting the expression of SLC7A11 so that AFT3 was a promoter of

ferroptosis induced by erastin[46]. In current study, we conformably found ATF3 was upregulated at Day 1, 3, 7, 14 and 56 after SCI and it was annotated as a driver of ferroptosis in FerrDb.

X-box binding protein 1 (XBP1) was first described in 1990[47], it is downstream of inositol-requiring enzyme 1 (IRE1α) and is a key transcription factor in the unfolded protein response (UPR)[48]. According to the literature, IRE1-XBP1 axis affected homeostasis of ER in oligodendrocyte and functional recovery after SCI[49]. Although XBP1 was demonstrated has a close link with ER stress and its accumulation also be seen at the injury epicenter after SCI [49], effects of XBP1 in ferroptosis is rare reported. Here, expression of XBP1 was increased at Day 1, 3, 7, 14 and 56 after SCI, the annotation of XBP1 in FerrDb was the marker of ferroptosis and may promote ferroptosis. Hence we reckoned that ER stress response might have the effect of bridge between XBP1 and ferroptosis, which provided a novel insight for deeper exploration of ferroptosis-related mechanism in SCI.

Heme Oxygenase 1 (HMOX1, HO-1) is critical to heme metabolism[50]. The function of HO-1 in ferroptosis is controversial, with studies reporting that it can either drive or suppress ferroptosis as it described in FerrDb [51]. It was reported that augmented level of HO-1 contributed to defense against ferroptosis in SCI[27, 28], which indicated that HO-1 might play the ferroptotic suppressor role in SCI. Moreover, HO-1 is present downstream of NFE2L2 (NRF2) and HO-1 expression is closely regulated by NFE2L2 [52] that was identified as a upregulated hub gene in our research.

DNA Damage Inducible Transcript 3 (DDIT 3), or named C/EBP homologous protein (CHOP), belongs to the family of CCAAT/enhancer binding proteins (C/EBPs) and regulates genes that encode proteins involved in proliferation, differentiation and expression, and energy metabolism[53]. Restraint of DDIT3 can promote functional recover of SCI via diminishing neuronal apoptosis[54] and preserving oligodendrocytes and axons[55]. DDIT3 is also involved in regulation of ferroptosis by affecting synthesis of intracellular GSH[56].

Gamma-GCT Acting On Glutathione Homolog 1 (CHAC1) is a newly discovered ER stress inducible gene, involved in Glutathione metabolism and cell apoptosis or ferroptosis[57]. CHAC1 can be triggered by depletion of glutathione and activation of ATF4 and expression of CHAC1 and ATF4 enhance the glutathione depletion in turn[58]. It is the feedforward mechanism that strengthen ferroptosis. CHAC1 was reported to upregulated at 1 day and 3 days post-SCI and attenuation of CHAC1 via CD36 knockout improved the vascularity within the injury region [59]. Notably, the improvements were observed at both 1 and 3 days post-injury but not by 7 weeks post-injury[59], which correspond to our results.

Conclusion

In this study, we constructed a contusive SCI model and ferroptotic phenotype was verified. Then, a comprehensive bioinformatic analysis was conducted based on GEO and FerrDb database. Ferroptotic DEGs were obtained at 5 time points (Day 1, 3, 7, 14, 56). The mTOR signaling pathway, VEGF signaling pathway, HIF-1 signaling pathway, protein processing in endoplasmic reticulum were essential in ferroptosis following SCI. Eventually, total twelve hub genes of five time points were identified by PPI network, among which *ATF3, XBP1, HMOX1, DDIT3, CHAC1* were differentially expressed in acute, subacute and chronic phase of SCI, thus they were considered as the key genes of ferroptosis following SCI. The expression of key genes in acute stage of SCI were verified. Nonetheless, further research in vivo and vitro should be undertaken to determine the role of ferroptosis in SCI. Collectively, the current study provides novel insights for further definition of precise molecular mechanism of ferroptosis signaling in SCI context, contributing to exploration of potential targets for SCI.

Declarations

Acknowledgements

We appreciate the basic laboratory facilities provided by the Key Laboratory of Microbiology and Parasitology of Anhui Province and the Key Laboratory of Zoonoses of High Institutions in Anhui.

Author Contribution

Yu Kang, Xuanming Shi and Zongsheng Yin designed the study. Yu Kang and Qiangwei Li performed the animal experiments and bioinformatic analysis together with the help of Rui Zhu, Shuang Li and Xin Xu. Rui Zhu performed HE, Nissl and Perls-blue stain.

Shuang Li performed the TEM test. Xin Xu performed the WB test. Yu Kang and Qiangwei Li wrote the manuscript. Rui Zhu, Shuang Li and Xin Xu contributed to data analysis and figures. All authors reviewed and concurred with the final manuscript. Yu Kang and Zongsheng Y took responsibility for the whole study

Funding

This study was supported by the National Natural Science Foundation of China (81871785 and 81672161).

Data Availability

The original contributions presented in the study are included in the article/supplementary material, further inquiries can be directed to the corresponding authors.

Ethics Approval and Consent to Participate

The study protocols regarding the animals were approved by the Ethics Committee of Anhui Medical University of China (No.LLSC 20201135).

Consent for Publication

Not applicable.

Conflict of Interest

The authors declare that the research was conducted in the absence of any commercial or financial relationships that could be construed as a potential conflict of interest.

References

1. Adams MM, Hicks AL (2005) Spasticity after spinal cord injury. Spinal Cord 43577–586. doi:10.1038/sj.sc.3101757
2. Vacca V, Madaro L, De Angelis F, Proietti D, Cobianchi S, Orsini T, Puri PL, Luvisetto S, Pavone F, Marinelli S (2020) Revealing the Therapeutic Potential of Botulinum Neurotoxin Type A in Counteracting Paralysis and Neuropathic Pain in Spinally Injured Mice. Toxins (Basel) 12(8):491. doi: 10.3390/toxins12080491
3. Chen Y, Liu S, Li J, Li Z, Quan J, Liu X, Tang Y, Liu B (2020) The Latest View on the Mechanism of Ferroptosis and Its Research Progress in Spinal Cord Injury. Oxid Med Cell Longev 6375938. doi: 10.1155/2020/6375938
4. Wu C, Xu H, Li J, Hu X, Wang X, Huang Y, Li Y, Sheng S, Wang Y, Xu H, Ni W, Zhou K (2020) Baicalein Attenuates Pyroptosis and Endoplasmic Reticulum Stress Following Spinal Cord Ischemia-Reperfusion Injury via Autophagy Enhancement. Front Pharmacol 11:1076. doi: 10.3389/fphar.2020.01076
5. Fan H, Tang HB, Shan LQ, Liu SC, Huang DG, Chen X, Chen Z, Yang M, Yin XH, Yang H, Hao DJ (2019) Quercetin prevents necroptosis of oligodendrocytes by inhibiting macrophages/microglia polarization to M1 phenotype after spinal cord injury in rats. J Neuroinflammation 16(1):206. doi: 10.1186/s12974-019-1613-2
6. Wang W, Huang X, Li J, Sun A, Yu J, Xie N, Xi Y, Ye X (2017) Methane Suppresses Microglial Activation Related to Oxidative, Inflammatory, and Apoptotic Injury during Spinal Cord Injury in Rats. Oxid Med Cell Longev 2190897. doi: 10.1155/2017/2190897
7. Dixon SJ, Lemberg KM, Lamprecht MR, Skouta R, Zaitsev EM, Gleason CE, Patel DN, Bauer AJ, Cantley AM, Yang WS, Morrison B 3rd (2012) Stockwell BR. Ferroptosis: an iron-dependent form of nonapoptotic cell death. Cell 149(5):1060–1072. doi: 10.1016/j.cell.2012.03.042
8. Shen L, Lin D, Li X, Wu H, Lenahan C, Pan Y, Xu W, Chen Y, Shao A, Zhang J (2020) Ferroptosis in Acute Central Nervous System Injuries: The Future Direction? Front Cell Dev Biol 8:594. doi: 10.3389/fcell.2020.00594
9. Zhang Y, Fan BY, Pang YL, Shen WY, Wang X, Zhao CX, Li WX, Liu C, Kong XH, Ning GZ, Feng SQ, Yao X (2020) Neuroprotective effect of deferoxamine on erastininduced ferroptosis in primary cortical neurons. Neural Regen Res 15(8):1539–1545. doi: 10.4103/1673-5374.274344

10. Zhang Y, Sun C, Zhao C, Hao J, Zhang Y, Fan B, Li B, Duan H, Liu C, Kong X, Wu P, Yao X, Feng S (2019) Ferroptosis inhibitor SRS 16-86 attenuates ferroptosis and promotes functional recovery in contusion spinal cord injury. Brain Res 1706:48–57. doi: 10.1016/j.brainres.2018.10.023
11. Yao X, Zhang Y, Hao J, Duan HQ, Zhao CX, Sun C, Li B, Fan BY, Wang X, Li WX, Fu XH, Hu Y, Liu C, Kong XH, Feng SQ (2019) Deferoxamine promotes recovery of traumatic spinal cord injury by inhibiting ferroptosis. Neural Regen Res 14(3):532–541. doi: 10.4103/1673-5374.245480
12. Barrett T, Wilhite SE, Ledoux P, Evangelista C, Kim IF, Tomashevsky M, Marshall KA, Phillippy KH, Sherman PM, Holko M, Yefanov A, Lee H, Zhang N, Robertson CL, Serova N, Davis S, Soboleva A (2013) NCBI GEO: archive for functional genomics data sets–update. Nucleic Acids Res. ; 41(Database issue): D991-5. doi: 10.1093/nar/gks1193
13. Zhou N, Bao J (2020) FerrDb: a manually curated resource for regulators and markers of ferroptosis and ferroptosis-disease associations. Database (Oxford). doi: 10.1093/database/baaa021
14. Zhong L, Zhang H, Ding ZF, Li J, Lv JW, Pan ZJ, Xu DX, Yin ZS (2020) Erythropoietin-Induced Autophagy Protects Against Spinal Cord Injury and Improves Neurological Function via the Extracellular-Regulated Protein Kinase Signaling Pathway. Mol Neurobiol 57(10):3993–4006. doi: 10.1007/s12035-020-01997-0
15. Basso DM, Beattie MS, Bresnahan JC (1995) A sensitive and reliable locomotor rating scale for open field testing in rats. J Neurotrauma 12(1):1–21. doi: 10.1089/neu.1995.12.1
16. Huang da W, Sherman BT, Lempicki RA (2009) Bioinformatics enrichment tools: paths toward the comprehensive functional analysis of large gene lists. Nucleic Acids Res 37(1):1–13. doi: 10.1093/nar/gkn923
17. Fang S, Zhong L, Wang AQ, Zhang H, Yin ZS (2021) Identification of Regeneration and Hub Genes and Pathways at Different Time Points after Spinal Cord Injury. Mol Neurobiol 58(6):2643–2662. doi: 10.1007/s12035-021-02289-x
18. Bu D, Luo H, Huo P, Wang Z, Zhang S, He Z, Wu Y, Zhao L, Liu J, Guo J, Fang S, Cao W, Yi L, Zhao Y, Kong L (2021) KOBAS-i: intelligent prioritization and exploratory visualization of biological functions for gene enrichment analysis. Nucleic Acids Res 49(W1):W317–W325. doi: 10.1093/nar/gkab447
19. Xu N, Cui Y, Dong J, Huang L (2020) Exploring the Molecular Mechanisms of Pterygium by Constructing lncRNA-miRNA-mRNA Regulatory Network. Invest Ophthalmol Vis Sci 61(8):12. doi: 10.1167/iovs.61.8.12
20. Subramanian A, Tamayo P, Mootha VK, Mukherjee S, Ebert BL, Gillette MA, Paulovich A, Pomeroy SL, Golub TR, Lander ES, Mesirov JP (2005) Gene set enrichment analysis: a knowledge-based approach for interpreting genome-wide expression profiles. Proc Natl Acad Sci U S A 102(43):15545–15550. doi: 10.1073/pnas.0506580102
21. Peng S, Yang S, Bo X, Li F (2017) paraGSEA: a scalable approach for large-scale gene expression profiling. Nucleic Acids Res 45(17):e155. doi: 10.1093/nar/gkx679
22. Szklarczyk D, Gable AL, Nastou KC, Lyon D, Kirsch R, Pyysalo S, Doncheva NT, Legeay M, Fang T, Bork P, Jensen LJ, von Mering C (2021) The STRING database in 2021: customizable protein-protein networks, and functional characterization of user-uploaded gene/measurement sets. Nucleic Acids Res 49(D1):D605–D612. doi: 10.1093/nar/gkaa1074
23. Shannon P, Markiel A, Ozier O, Baliga NS, Wang JT, Ramage D, Amin N, Schwikowski B, Ideker T (2003) Cytoscape: a software environment for integrated models of biomolecular interaction networks. Genome Res 13(11):2498–2504. doi: 10.1101/gr.1239303
24. Chamankhah M, Eftekharpour E, Karimi-Abdolrezaee S, Boutros PC, San-Marina S, Fehlings MG Genome-wide gene expression profiling of stress response in a spinal cord clip compression injury model.BMC Genomics. 2013 Aug28;14:583. doi: 10.1186/1471-2164-14-583
25. Wang W, Su Y, Tang S, Li H, Xie W, Chen J, Shen L, Pan X, Ning B (2019) Identification of noncoding RNA expression profiles and regulatory interaction networks following traumatic spinal cord injury by sequence analysis. Aging 11(8):2352–2368. doi: 10.18632/aging.101919
26. Yao XQ, Liu ZY, Chen JY, Huang ZC, Liu JH, Sun BH, Zhu QA, Ding RT, Chen JT (2021) Proteomics and bioinformatics reveal insights into neuroinflammation in the acute to subacute phases in rat models of spinal cord contusion injury. FASEB J 35(7):e21735. doi: 10.1096/fj.202100081RR
27. Zhou H, Yin C, Zhang Z, Tang H, Shen W, Zha X, Gao M, Sun J, Xu X, Chen Q (2020) Proanthocyanidin promotes functional recovery of spinal cord injury via inhibiting ferroptosis. J Chem Neuroanat 107:101807. doi: 10.1016/j.jchemneu.2020.101807

28. Ge MH, Tian H, Mao L, Li DY, Lin JQ, Hu HS, Huang SC, Zhang CJ, Mei XF (2021) Zinc attenuates ferroptosis and promotes functional recovery in contusion spinal cord injury by activating Nrf2/GPX4 defense pathway. CNS Neurosci Ther 27(9):1023–1040. doi: 10.1111/cns.13657
29. Kanno H, Ozawa H, Sekiguchi A, Yamaya S, Tateda S, Yahata K, Itoi E (2012) The role of mTOR signaling pathway in spinal cord injury. Cell Cycle 11(17):3175–3179. doi: 10.4161/cc.21262
30. Chen H, Xu G, Wu Y, Wang X, Wang F, Zhang Y (2021) HBO-PC Promotes Locomotor Recovery by Reducing Apoptosis and Inflammation in SCI Rats: The Role of the mTOR Signaling Pathway. Cell Mol Neurobiol 41(7):1537–1547. doi: 10.1007/s10571-020-00921-3
31. Liu Y, Wang Y, Liu J, Kang R, Tang D (2021) Interplay between MTOR and GPX4 signaling modulates autophagy-dependent ferroptotic cancer cell death. Cancer Gene Ther 28(1–2):55–63. doi: 10.1038/s41417-020-0182-y
32. Han X, Chen Y, Liu Y, Wang Z, Tang G, Tian W (2018) HIF-1α promotes bone marrow stromal cell migration to the injury site and enhances functional recovery after spinal cord injury in rats. J Gene Med 20(12):e3062. doi: 10.1002/jgm.3062
33. Luo Z, Wu F, Xue E, Huang L, Yan P, Pan X, Zhou Y (2019) Hypoxia preconditioning promotes bone marrow mesenchymal stem cells survival by inducing HIF-1α in injured neuronal cells derived exosomes culture system. Cell Death Dis 10(2):134. doi: 10.1038/s41419-019-1410-y
34. Yang M, Chen P, Liu J, Zhu S, Kroemer G, Klionsky DJ, Lotze MT, Zeh HJ, Kang R, Tang D (2019) Clockophagy is a novel selective autophagy process favoring ferroptosis. Sci Adv 5(7):eaaw2238. doi: 10.1126/sciadv.aaw2238
35. Chen H, Li J, Liang S, Lin B, Peng Q, Zhao P, Cui J, Rao Y (2017) Effect of hypoxia-inducible factor-1/vascular endothelial growth factor signaling pathway on spinal cord injury in rats. Exp Ther Med 13(3):861–866. doi: 10.3892/etm.2017.4049
36. Zhao X, Gao M, Liang J, Chen Y, Wang Y, Wang Y, Xiao Y, Zhao Z, Wan X, Jiang M, Luo X, Wang F, Sun X (2021) SLC7A11 Reduces Laser-Induced Choroidal Neovascularization by Inhibiting RPE Ferroptosis and VEGF Production. Front Cell Dev Biol 9:639851. doi: 10.3389/fcell.2021.639851
37. Oakes SA, Papa FR (2015) The role of endoplasmic reticulum stress in human pathology. Annu Rev Pathol 10:173–194. doi: 10.1146/annurev-pathol-012513-104649
38. Huang C, Zhang W, Chu F, Qian H, Wang Y, Qi F, Ye M, Zhou J, Lin Z, Dong C, Wang X, Wang Q, Jin H (2021) Patchouli Alcohol Improves the Integrity of the Blood-Spinal Cord Barrier by Inhibiting Endoplasmic Reticulum Stress Through the Akt/CHOP/Caspase-3 Pathway Following Spinal Cord Injury. Front Cell Dev Biol 9:693533. doi: 10.3389/fcell.2021.693533
39. McGrath EP, Centonze FG, Chevet E, Avril T, Lafont E (2021) Death sentence: The tale of a fallen endoplasmic reticulum. Biochim Biophys Acta Mol Cell Res 1868(6):119001. doi: 10.1016/j.bbamcr.2021.119001
40. Dixon SJ, Patel DN, Welsch M, Skouta R, Lee ED, Hayano M, Thomas AG, Gleason CE, Tatonetti NP, Slusher BS, Stockwell BR (2014) Pharmacological inhibition of cystine-glutamate exchange induces endoplasmic reticulum stress and ferroptosis. Elife 3:e02523. doi: 10.7554/eLife.02523
41. Rahmani M, Davis EM, Crabtree TR, Habibi JR, Nguyen TK, Dent P, Grant S (2007) The kinase inhibitor sorafenib induces cell death through a process involving induction of endoplasmic reticulum stress. Mol Cell Biol 27(15):5499–5513. doi: 10.1128/MCB.01080-06
42. Chen D, Fan Z, Rauh M, Buchfelder M, Eyupoglu IY, Savaskan N (2017) ATF4 promotes angiogenesis and neuronal cell death and confers ferroptosis in a xCT-dependent manner. Oncogene 36(40):5593–5608. doi: 10.1038/onc.2017.146
43. Sarcinelli C, Dragic H, Piecyk M, Barbet V, Duret C, Barthelaix A, Ferraro-Peyret C, Fauvre J, Renno T, Chaveroux C, Manié SN (2020) ATF4-Dependent *NRF2* Transcriptional Regulation Promotes Antioxidant Protection during Endoplasmic Reticulum Stress. Cancers (Basel) 12(3):569. doi: 10.3390/cancers12030569
44. Hai T, Wolfgang CD, Marsee DK, Allen AE, Sivaprasad U (1999) ATF3 and stress responses. Gene Expr 7(4–6):321–335
45. Huang WL, George KJ, Ibba V, Liu MC, Averill S, Quartu M, Hamlyn PJ, Priestley JV (2007) The characteristics of neuronal injury in a static compression model of spinal cord injury in adult rats. Eur J Neurosci 25(2):362–372. doi: 10.1111/j.1460-9568.2006.05284.x
46. Wang L, Liu Y, Du T, Yang H, Lei L, Guo M, Ding HF, Zhang J, Wang H, Chen X, Yan C (2020) ATF3 promotes erastin-induced ferroptosis by suppressing system Xc. Cell Death Differ 27(2):662–675. doi: 10.1038/s41418-019-0380-z

47. Liou HC, Boothby MR, Finn PW, Davidon R, Nabavi N, Zeleznik-Le NJ, Ting JP, Glimcher LH (1990) A new member of the leucine zipper class of proteins that binds to the HLA DR alpha promoter. Science 247(4950):1581–1584. doi: 10.1126/science.2321018
48. Chen S, Chen J, Hua X, Sun Y, Cui R, Sha J, Zhu X (2020) The emerging role of XBP1 in cancer. Biomed Pharmacother 127:110069. doi: 10.1016/j.biopha.2020.110069
49. Saraswat Ohri S, Howard RM, Liu Y, Andres KR, Shepard CT, Hetman M, Whittemore SR (2021) Oligodendrocyte-specific deletion of Xbp1 exacerbates the endoplasmic reticulum stress response and restricts locomotor recovery after thoracic spinal cord injury. Glia 69(2):424–435. doi: 10.1002/glia.23907
50. Chiang SK, Chen SE, Chang LC (2018) A Dual Role of Heme Oxygenase-1 in Cancer Cells. Int J Mol Sci 20(1):39. doi: 10.3390/ijms20010039
51. Lettieri-Barbato D, Minopoli G, Caggiano R, Izzo R, Santillo M, Aquilano K, Faraonio R (2020) Fasting Drives Nrf2-Related Antioxidant Response in Skeletal Muscle. Int J Mol Sci 21(20):7780. doi: 10.3390/ijms21207780
52. Alam MB, Chowdhury NS, Sohrab MH, Rana MS, Hasan CM, Lee SH (2020) Cerevisterol Alleviates Inflammation via Suppression of MAPK/NF-κB/AP-1 and Activation of the Nrf2/HO-1 Signaling Cascade. Biomolecules 10(2):199. doi: 10.3390/biom10020199
53. Hu H, Tian M, Ding C, Yu S (2019) The C/EBP Homologous Protein (CHOP) Transcription Factor Functions in Endoplasmic Reticulum Stress-Induced Apoptosis and Microbial Infection. Front Immunol 9:3083. doi: 10.3389/fimmu.2018.03083
54. Gu C, Li H, Wang C, Song X, Ding Y, Zheng M, Liu W, Chen Y, Zhang X, Wang L (2017) Bone marrow mesenchymal stem cells decrease CHOP expression and neuronal apoptosis after spinal cord injury. Neurosci Lett 636:282–289. doi: 10.1016/j.neulet.2016.11.032
55. Penas C, Verdú E, Asensio-Pinilla E, Guzmán-Lenis MS, Herrando-Grabulosa M, Navarro X, Casas C (2011) Valproate reduces CHOP levels and preserves oligodendrocytes and axons after spinal cord injury. Neuroscience 178:33–44. doi: 10.1016/j.neuroscience.2011.01.012
56. Wang N, Zeng GZ, Yin JL, Bian ZX (2019) Artesunate activates the ATF4-CHOP-CHAC1 pathway and affects ferroptosis in Burkitt's Lymphoma. Biochem Biophys Res Commun 519(3):533–539. doi: 10.1016/j.bbrc.2019.09.023
57. Li D, Liu S, Xu J, Chen L, Xu C, Chen F, Xu Z, Zhang Y, Xia S, Shao Y, Wang Y (2021) Ferroptosis-related gene CHAC1 is a valid indicator for the poor prognosis of kidney renal clear cell carcinoma. J Cell Mol Med 25(7):3610–3621. doi: 10.1111/jcmm.16458
58. Ratan RR (2020) The Chemical Biology of Ferroptosis in the Central Nervous System. Cell Chem Biol 27(5):479–498. doi: 10.1016/j.chembiol.2020.03.007
59. Myers SA, Andres KR, Hagg T, Whittemore SR (2014) CD36 deletion improves recovery from spinal cord injury. Exp Neurol 256:25–38. doi: 10.1016/j.expneurol.2014.03.016

Tables

TABLE 1 Numbers of DEGs at each time point

Time points	Upregulated	Downregulated	Total
Day 1	23	14	37
Day 3	31	12	43
Day 7	18	10	28
Day 14	15	13	28
Day 56	19	13	32

TABLE 2 KEGG pathways analysis of DEGs

KEGG Term	Time Point	Gene	P Value
mTOR signaling pathway	Day 1	Slc3a2, Ddit4, Atp6v1g2, Sesn2	0.001
	Day 3	Slc3a2, Ddit4, Atp6v1g2, Sesn2	0.0005
	Day 7	Slc3a2, Atp6v1g2, Sesn2	0.006
	Day 14	Slc3a2, Ddit4, ATP6v1g2, Sesn2	8.49E-05
	Day 56	Slc3a2, Atp6v1g2, Sesn2	0.006
HIF-1 signaling pathway	Day 1	Vegfa, Rela, Hmox1	0.004
	Day 3	IL6, Tfrc, Hmox1, Slc2a1	0.0002
	Day 7	Vegfa, Rela, Hmox1	0.004
	Day 14	Vegfa, Tfrc, Hmox1	0.001
	Day 56	Vegfa, Tfrc, Hmox1	0.004
Ferroptosis	Day 3	Slc3a2, Tfrc, Hmox1	0.0003
	Day 7	Slc3a2, Hmox1	0.007
	Day 14	Slc3a2, Tfrc, Hmox1	8.49E-05
	Day 56	Slc3a2, Tfrc, Hmox1, Slc7a11	1.03E-05
VEGF signaling pathway	Day 1	Ptgs2, Vegfa, Hspb1	0.001
	Day 3	Mapk14, Ptgs2, Hspb1	0.0006
	Day 14	Vegfa, Hspb1	0.007
	Day 56	Vegfa, Hspb1	0.014
Protein processing in endoplasmic reticulum	Day 7	Nfe2l2, Eif2s1, Xbp1	0.005
	Day 14	Ddit3, Xbp1	0.02
	Day 56	Nfe2l2, Ddit3, Atf4, Xbp1	0.001

TABLE 3 Key Genes for Ferroptosis Regulation in SCI

Gene	Fullname	Description	Protein Encoded	Regulation of Ferroptosis	Expression	LogFC	Time Point
Atf3	Activating Transcription Factor 3	the complex process of cellular stress response	Cyclic AMP-dependent transcription factor ATF-3	Driver of ferroptosis	Upregulated	6.10	Day 1
					Upregulated	6.24	Day 3
					Upregulated	5.31	Day 7
					Upregulated	5.50	Day 14
					Upegulated	5.43	Day 56
Xbp1	X-box binding protein 1	Functions as a transcription factor during endoplasmic reticulum (ER) stress by regulating the unfolded protein response (UPR)	X-box-binding protein 1	May promote ferroptosis	Upregulated	1.09	Day 1
					Upregulated	0.91	Day 3
					Upregulated	0.90	Day 7
					Upregulated	0.72	Day 14
					Upregulated	0.82	Day 56
Hmox1 (HO-1)	Heme Oxygenase 1	Protein homodimerization activity and oxidoreductase activity	Heme oxygenase 1	Driver and Suppressor of ferroptosis	Upregulated	8,87	Day 1
					Upregulated	6,52	Day 7
					Upregulated	5.24	Day 14
					Upregulated	5.07	Day 56
Ddit3 (CHOP)	DNA Damage Inducible Transcript 3	activated by endoplasmic reticulum stress, and promotes apoptosis	DDIT3 upstream open reading frame protein	May promote ferroptosis	Upregulated	1.09	Day 3
					Upregulated	0.80	Day 14
					Upregulated	1.11	Day 56
Chac1	Gamma-GCT Acting On Glutathione Homolog 1	Metabolism and Glutathione metabolism, transferase activity, transferring acyl groups and Notch binding	Glutathione-specific gamma-glutamylcyclotransferase 1	Driver of ferroptosis	Upregulated	3.47	Day 3
					Downregulated	1.06	Day 14
					Downregulated	1.70	Day 56

Figures

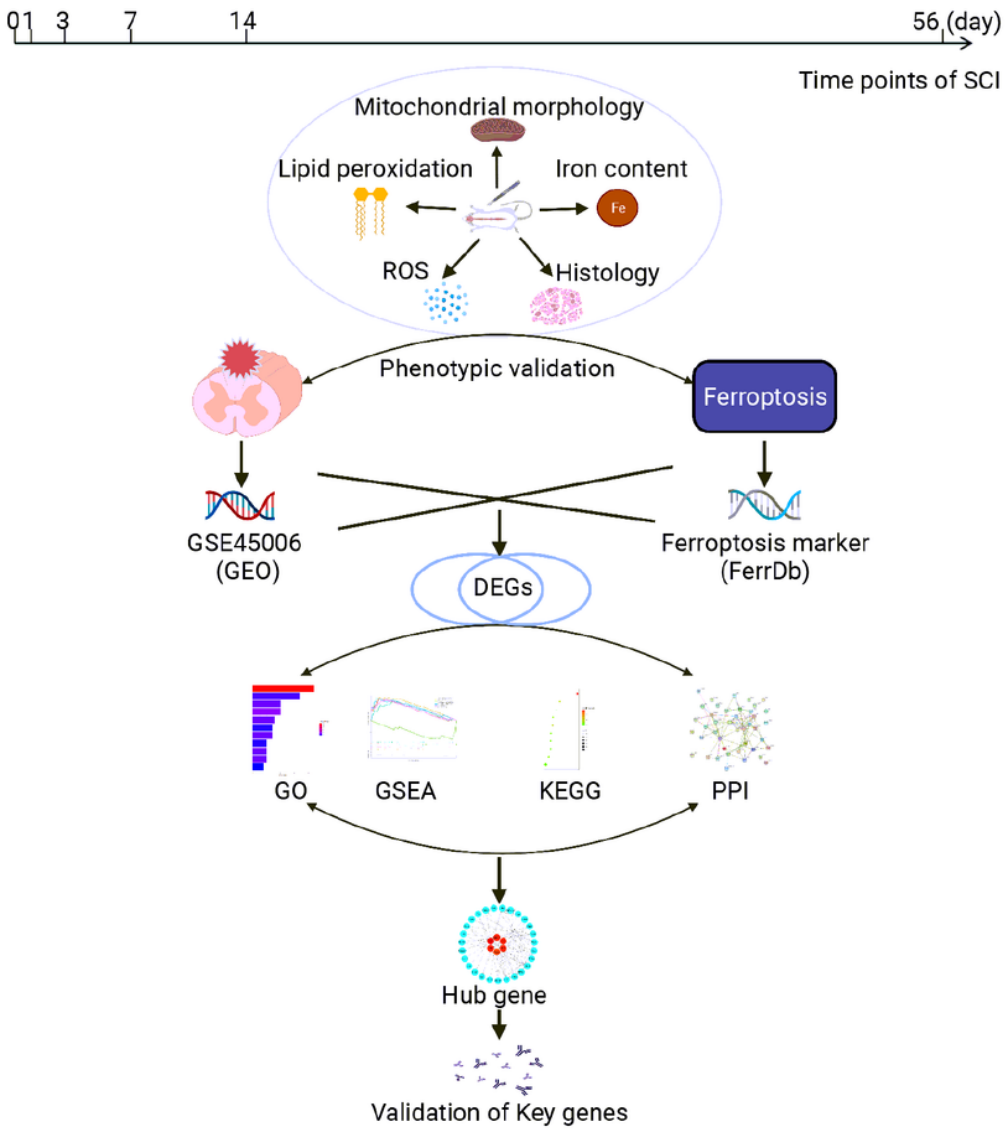

Figure 1

Schematic of the experimental strategy used to validate ferroptotic phenotype, identify hub genes and verify expression level of key genes.

Figure 2

Construction of SCI animal model and accumulation of tissue iron. (A, B, C) HE, Nissl and Perls-Blue staining for spinal cords of sham group, SCI_Day 3 group and SCI_Day 14 group (n=3). (D) BBB score of experimental animal at 1 day, 3 days, 7 days, 14 days after laminectomy and SCI (n=5). (E) Tissue iron content of sham group, SCI_Day 3 group and SCI_Day 14 group (n=5). Bar graphs show mean ± SD. P-values: T-test and One-way ANOVA analysis. (***p < 0.001)

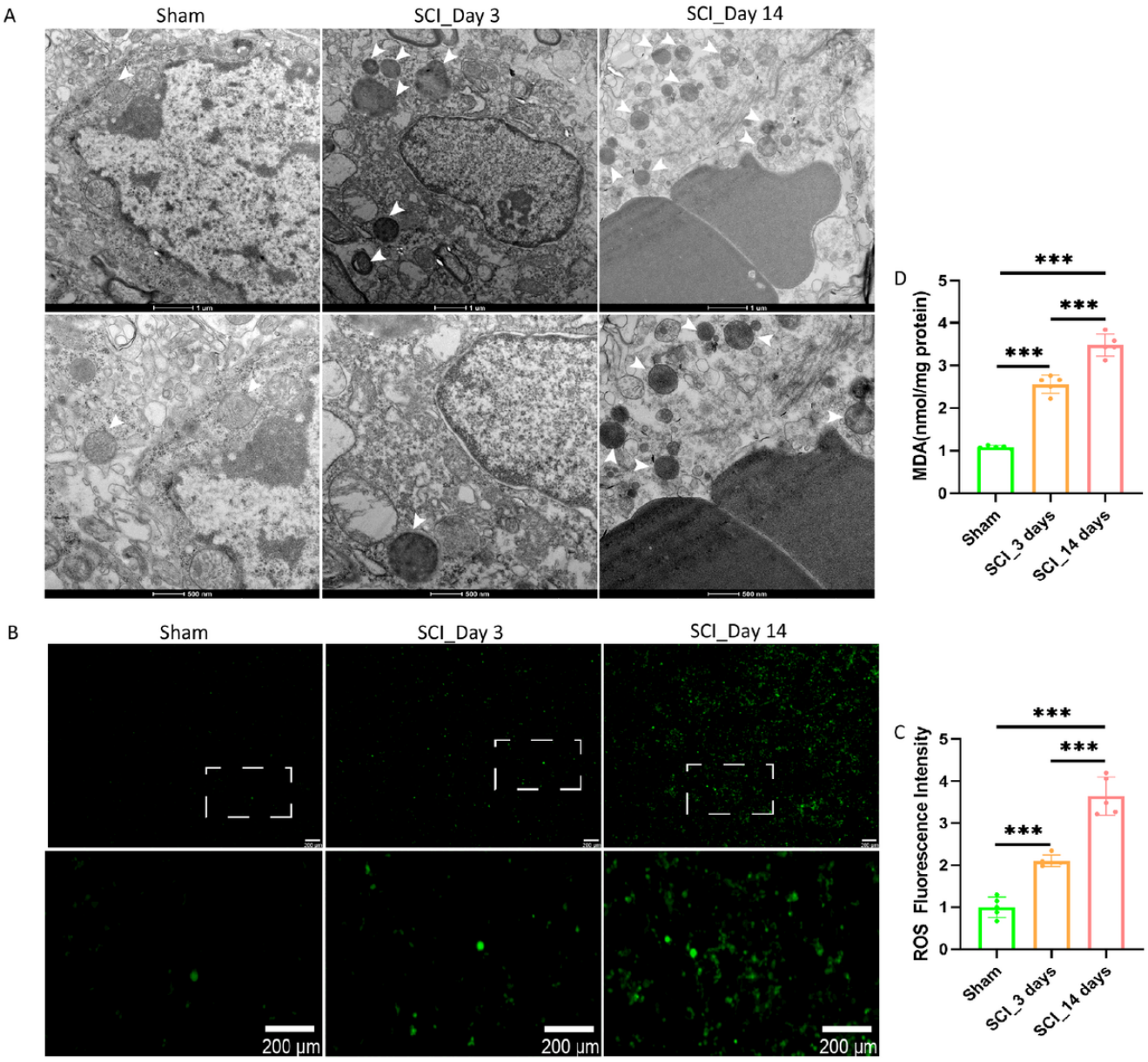

Figure 3

Observation of shrunken mitochondria and higher level of oxidation in SCI. (A) TEM was used to examine the ultrastructure of tissues after SCI. Shrunken mitochondria could be seen from SCI groups (Day 3 and Day 14) compared with Sham group. (B, C) Fluorescence imaging of ROS and the average intensity of fluorescence imaging by Image-J at sham group and 2 points in time after SCI (n = 5). (D) MDA, one of the products of lipid peroxidation, was augmented at SCI groups (Day 3 and Day 14) compared with Sham group (n = 5). Bar graphs show mean ± SD. P-values: One-way ANOVA analysis. (***p < 0.001).

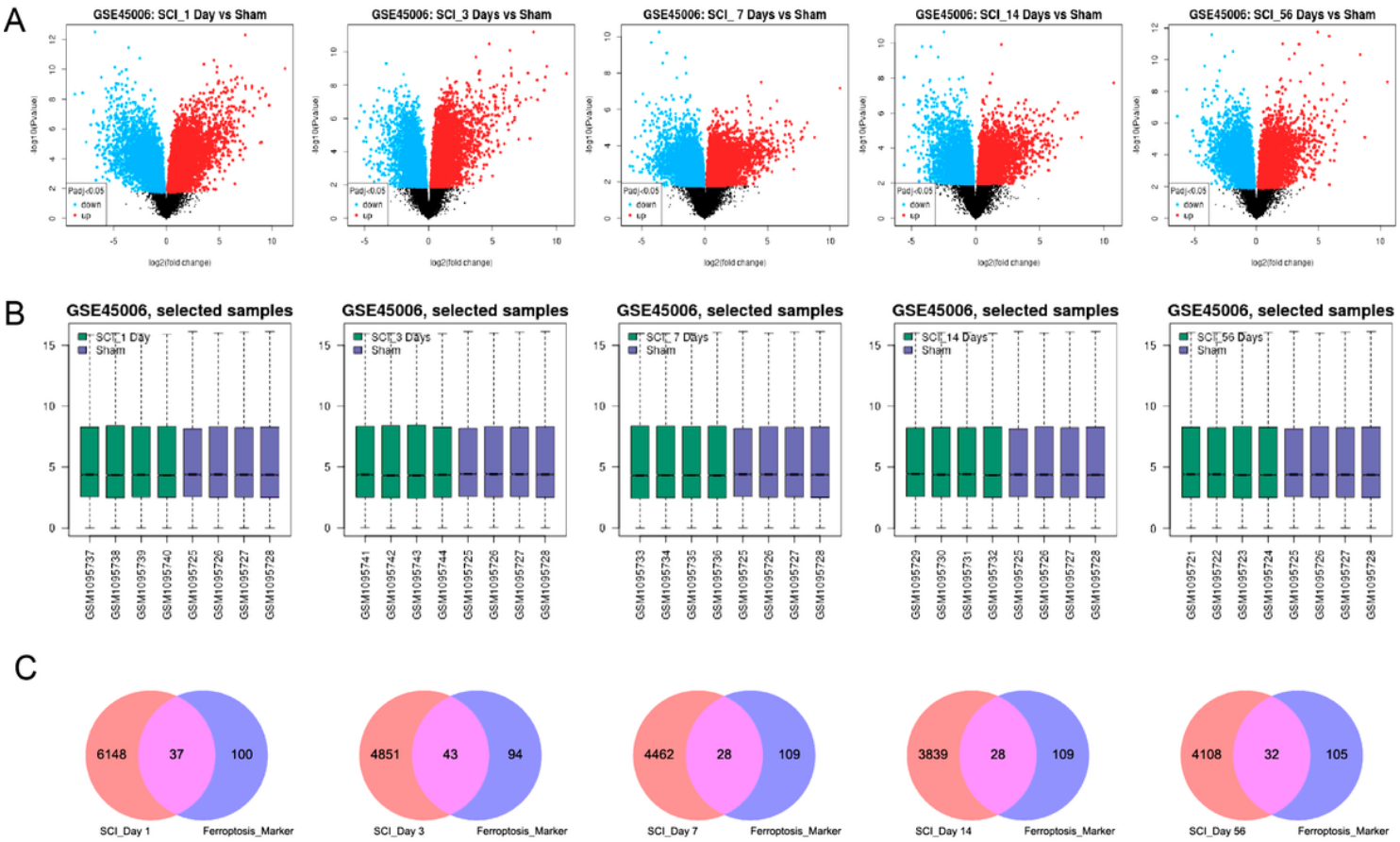

Figure 4

DEGs of each time point. (A) Volcano plot for genes between the SCI groups and sham group. Red plots represent upregulated genes. Blue plots represent downregulated genes. Black plots represent the genes with no significant difference. (B) The boxplots for microarray data in each time point (1 day/3 days/7 days/14 days/56days). The abscissa displays the samples, and the ordinate represents gene expression. (C) Venn diagrams of DEGs (Intersection of the ferroptosis markers and the genes with adjusted P-value < 0.05 and |logFC| ≥ 0.5).

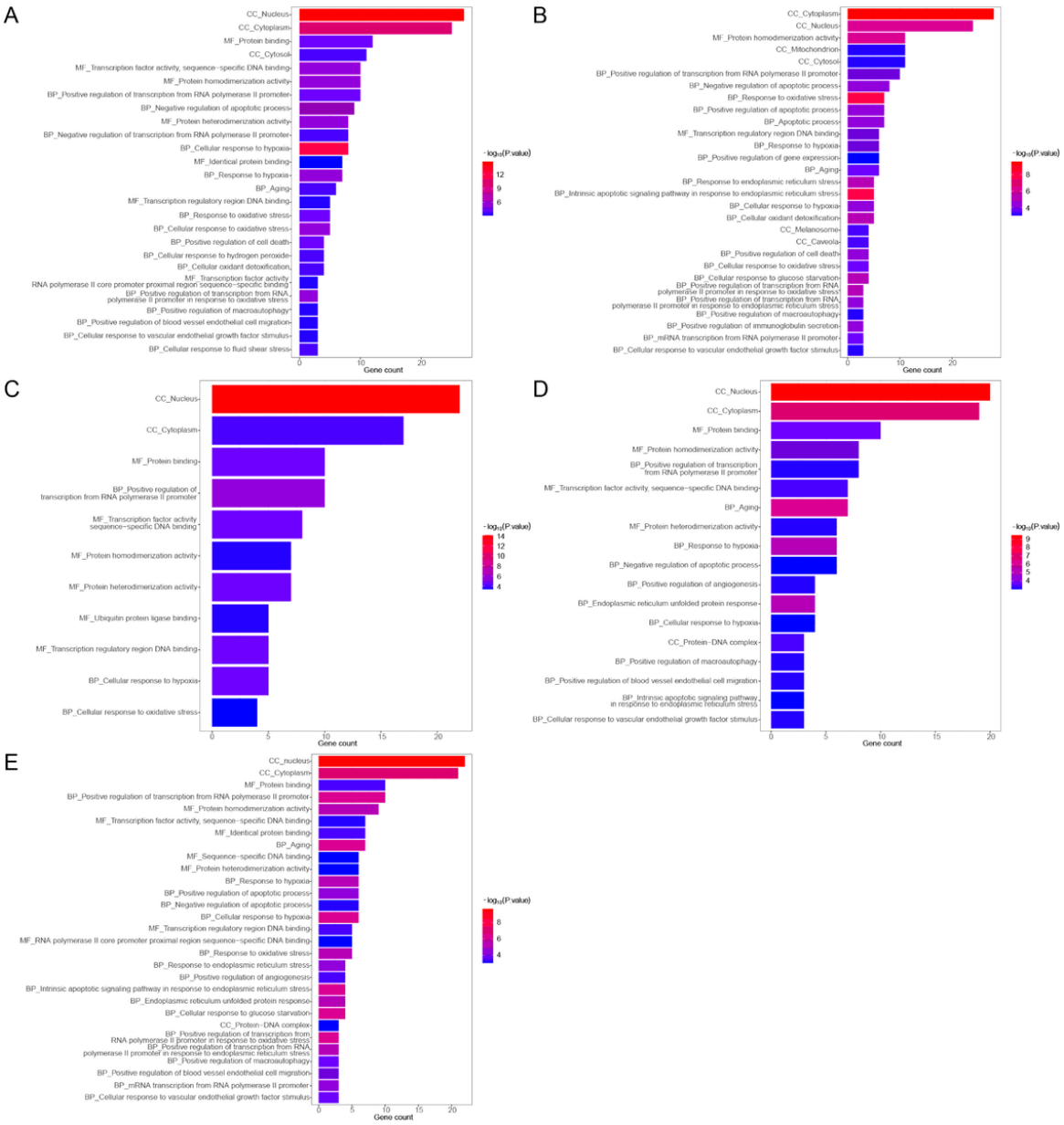

Figure 5

GO enrichment analysis for DEGs in 1 day (A), 3 days (B), 7 days (C), 14 days (D) and 56 days (E). The abscissa displays the gene count, the ordinate represents GO terms, the the color indicates the adjusted P-value.

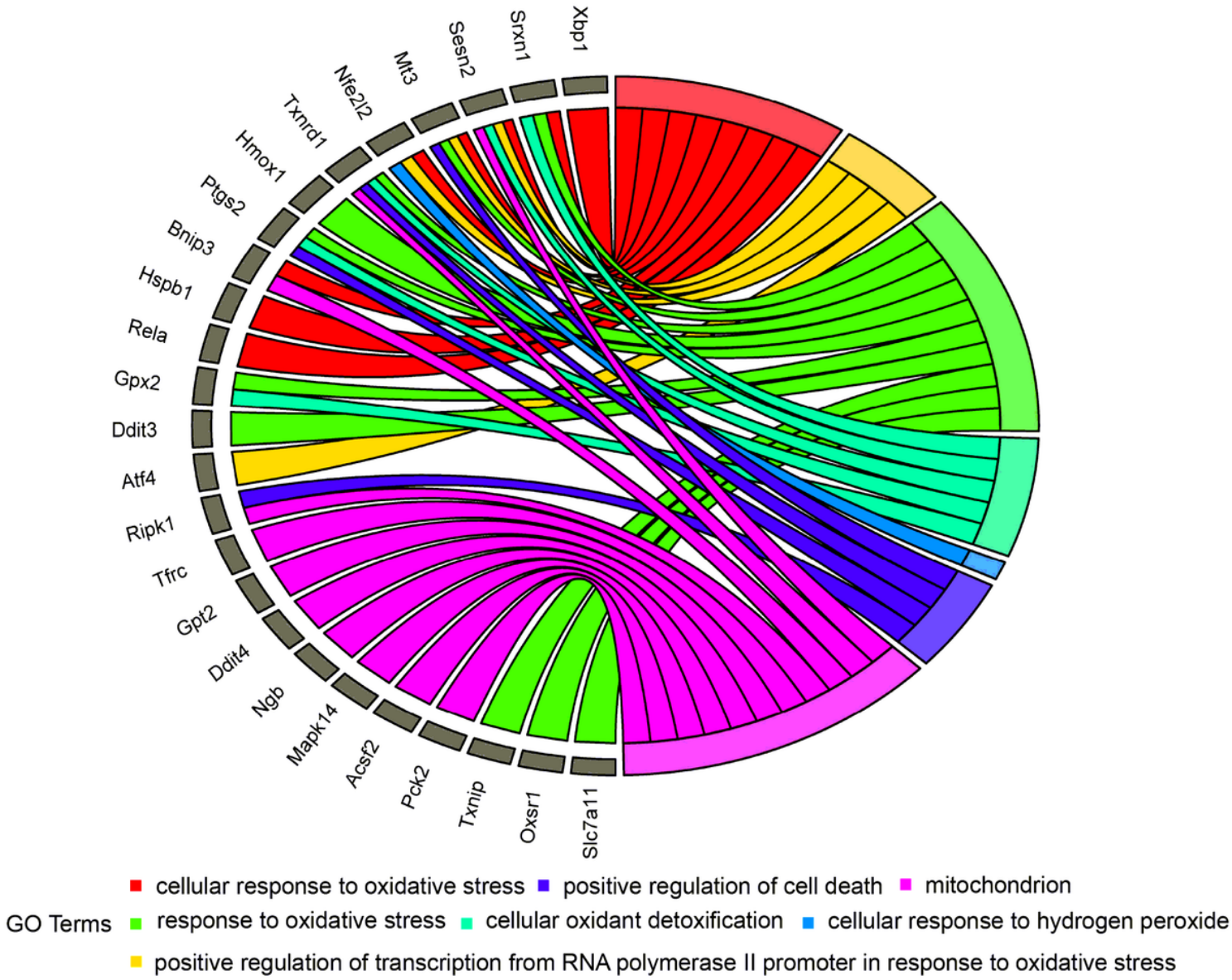

Figure 6

GO Chord plot; the genes are linked via oxidation, peroxidation, cell death and mitochondrion terms

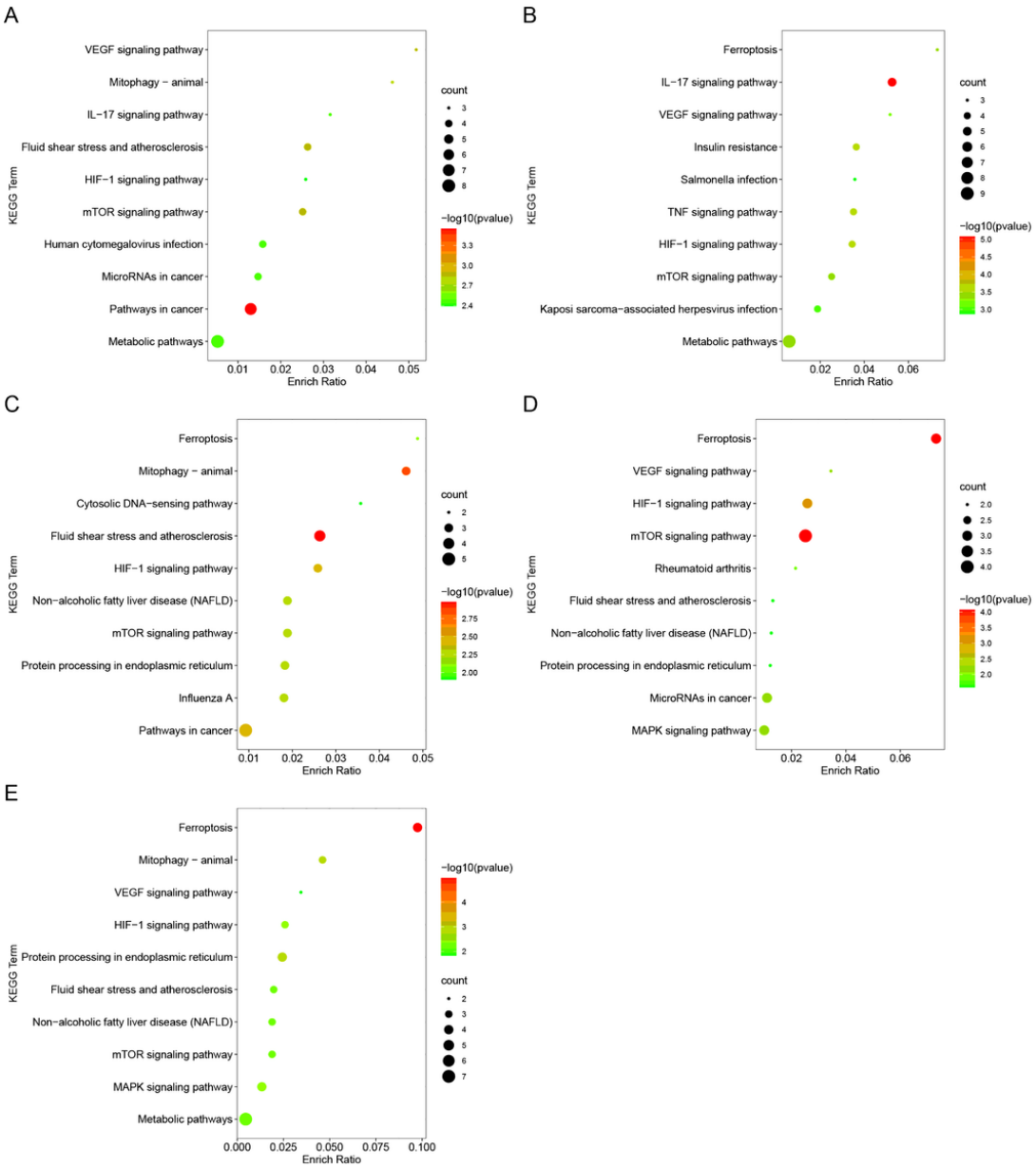

Figure 7

Top 10 KEGG pathways for DEGs in 1 day (A), 3 days (B), 7 days (C), 14 days (D) and 56 days (E). The abscissa displays the enrich ratio, the ordinate represents KEGG terms, The dots' size represents the number of enriched genes, and the color indicates the adjusted P-value.

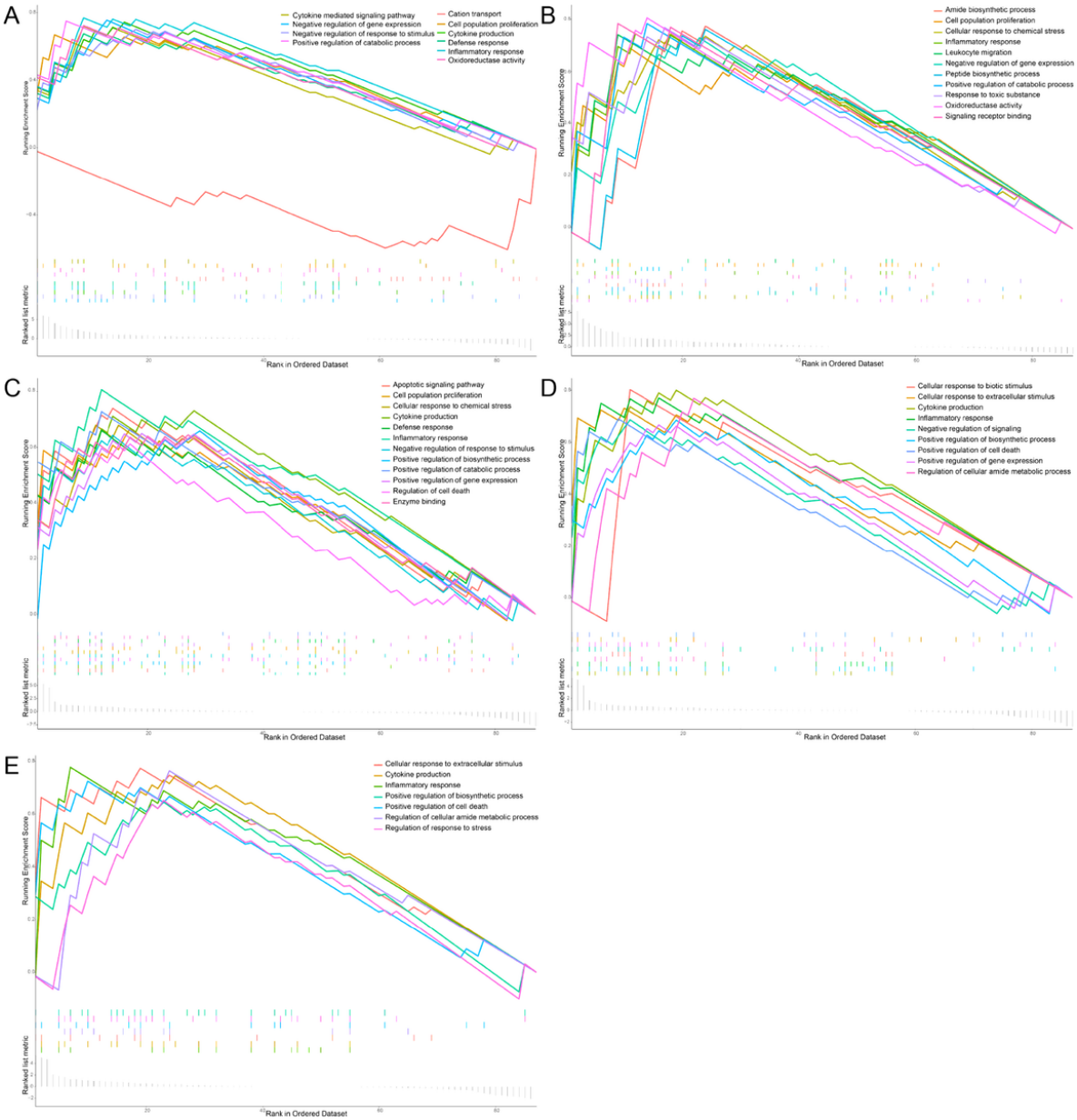

Figure 8

GSEA for 1 day (A), 3 days (B), 7 days (C), 14 days (D) and 56 days (E). Only terms with the p-value < .05 and NES > 1 were pictured.

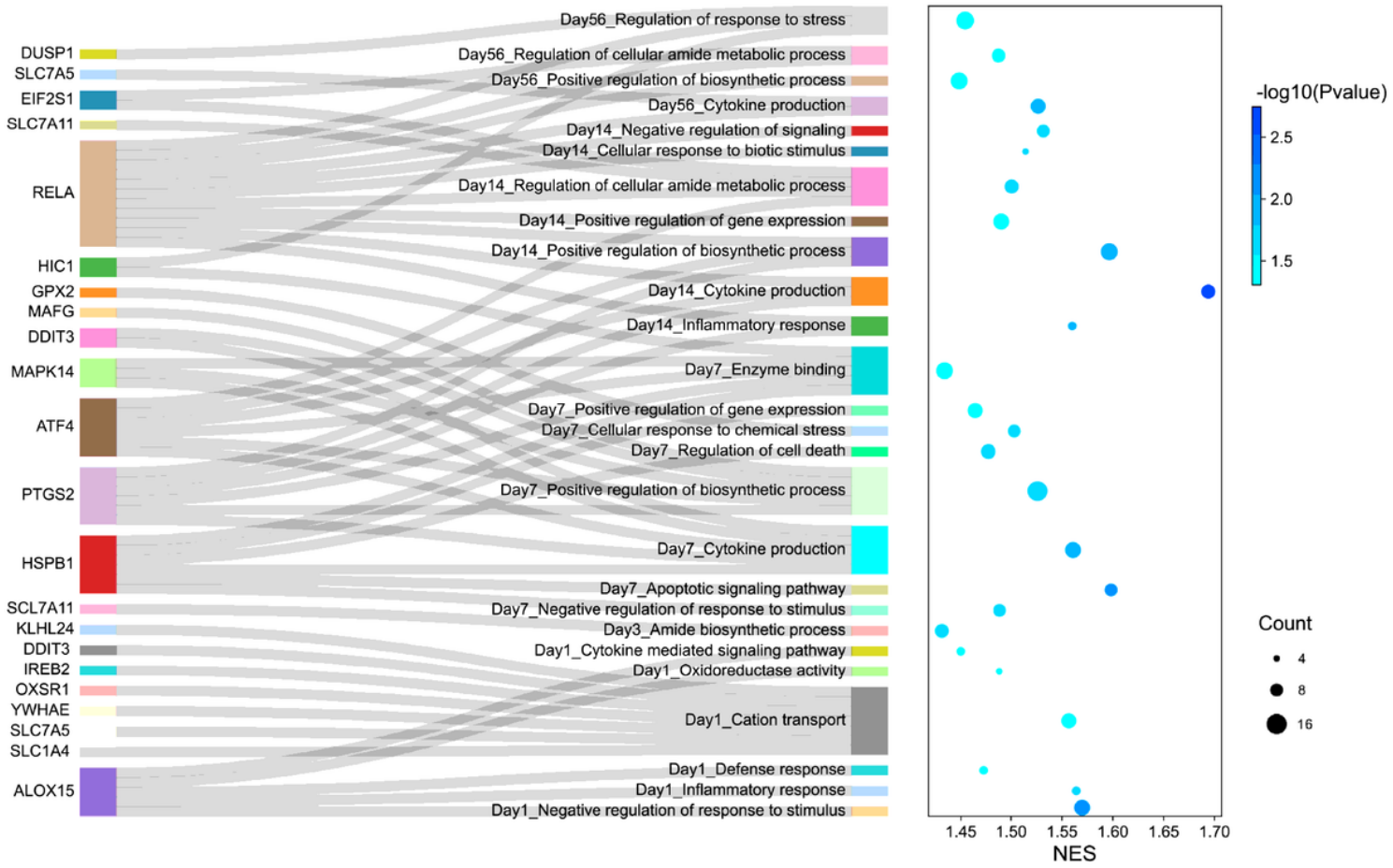

Figure 9

GSEA Sankey and dot plot; the non-DEGs in the leading edge subset and terms enriched by these genes were showed. The abscissa displays the NES, the ordinate represents GSEA terms, The dots' size represents the sum of enriched genes, and the the color indicates the P-value.

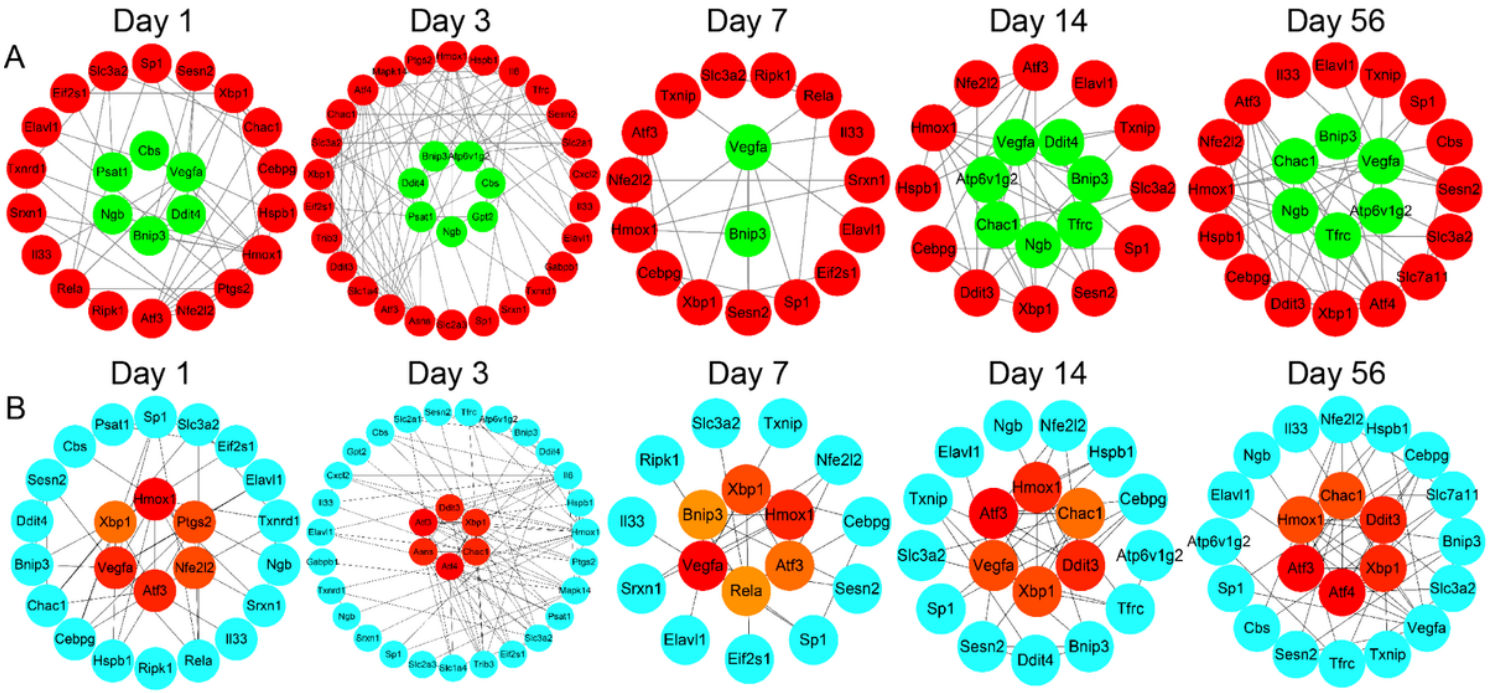

Figure 10

PPI network and hub genes.(A) PPI networks of 5 time points, Red means upregulated and green means downregulated. (B) Top 6 hub genes using MCC algorithm of 5 time points.

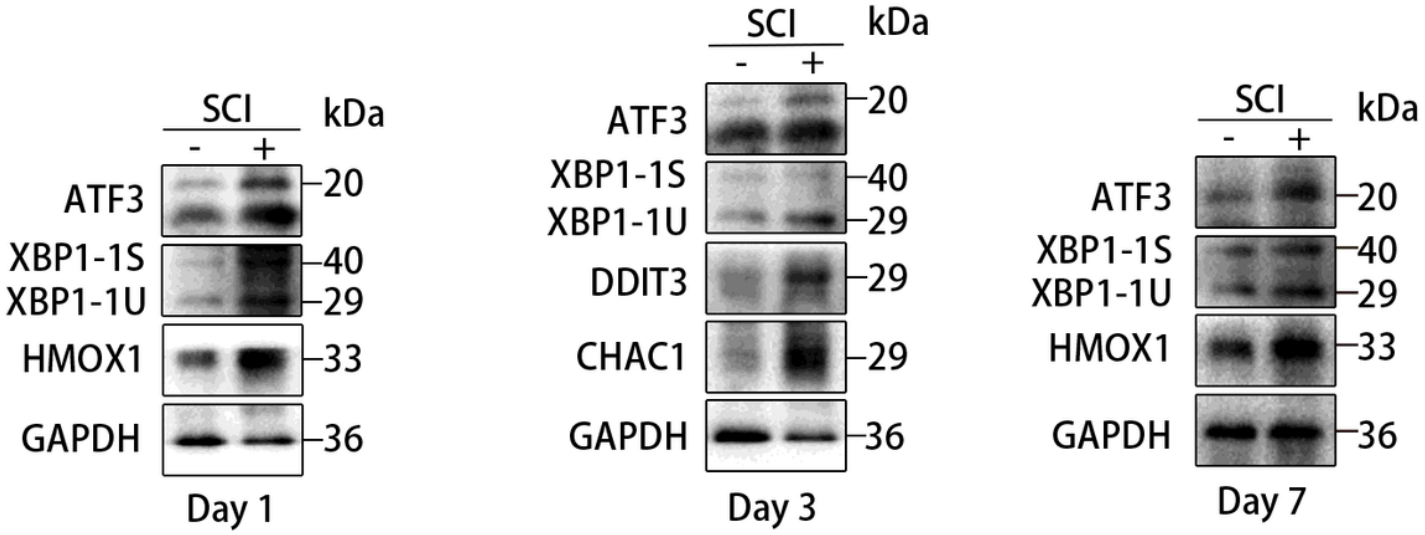

Figure 11

The expression validation of key genes after SCI, ATF3/XBP1/HMOX1 upregulated in day 1, ATF3/XBP1/DDIT3/CHAC1 upregulated in day 3, ATF3/XBP1/HMOX1 upregulated in day 7 (n=3).

Supplementary Files

This is a list of supplementary files associated with this preprint. Click to download.

- SupplementaryFigure1.pdf
- SupplementaryTable1.pdf
- SupplementaryTable2.pdf